

Exploring the Dark Age: Star and Galaxy formation in the Early Universe

K. El Bourakadi ^{1,2,*} and G. Otalora ^{1,†}

¹*Departamento de Física, Facultad de Ciencias, Universidad de Tarapacá, Casilla 7-D, Arica, Chile.*

²*Subatomic Research and Applications Team, Faculty of Science Ben M'sik, Casablanca Hassan II University, Morocco.*

(Dated: December 24, 2024)

The Cosmic Dark Ages mark a pivotal era of the universe's evolution, transitioning from a neutral, opaque medium to the emergence of the first stars and galaxies that initiated cosmic reionization. This study examines the thermodynamics of the intergalactic medium (IGM), molecular hydrogen cooling, and gravitational collapse that led to structure formation. Key emission lines, such as Lyman-alpha ($\text{Ly}\alpha$) and [C II] $158 \mu\text{m}$, are analyzed as tracers of star formation, metallicity, and IGM conditions. Simulations highlight $\text{Ly}\alpha$ scattering profiles and [C II] emission as critical diagnostics of early galaxy evolution. The findings provide a theoretical framework to interpret high-redshift observations, advancing our understanding of the universe's transition from darkness to illumination.

I. INTRODUCTION

Observations from cutting-edge telescopes across γ -ray to radio wavelengths, astronomers are now uncovering galaxies, Active Galactic Nuclei (AGN), which trace back to roughly 500–940 million years following the Big Bang [1]. This period marks the era of "cosmic reionization," during which radiation from the first galaxies and black holes reionized the neutral InterGalactic Medium (IGM) that dominated the universe after recombination. Observational evidence, such as data from the cosmic microwave background [2], the Gunn–Peterson trough in the spectra of quasars at $z > 6$ [3], the characteristics of $\text{Ly}\alpha$ emission in galaxies at similar redshifts [4], and constraints on the 21 cm signal from the neutral IGM [4, 6], has increasingly refined the timeline of reionization. It is now evident that the transformation of the IGM from predominantly neutral to highly ionized occurred primarily between redshifts $z \sim 6$ and 10, driven by the emergence of early galaxies [7–9]. The next decade promises significant advancements in understanding this critical phase of cosmic evolution, thanks to the James Webb Space Telescope (JWST), upcoming 30-meter-class ground-based telescopes for optical and near-infrared studies, and the expanded capabilities of the Atacama Large Millimeter Array (ALMA) across its full frequency range. These cutting-edge tools are set to provide unprecedented insights into this pivotal era.

The universe at $z \sim 15$ represents a frontier in our current understanding of cosmic evolution. Few theoretical investigations have explored the Star Formation Rate (SFR) density at these extreme redshifts, often in the context of early reionization [10–14]. Unlike galaxy formation at lower redshifts, early structures are thought to have significantly lower dynamical masses, making them more vulnerable to supernova feedback, which could inhibit or completely halt star formation by ejecting or heating their gas. Additionally, radiative feedback from nearby sources producing photoionizing radiation increases the Jeans length in the intergalactic medium, preventing the formation of the smallest galaxies with circular velocities below $\sim 50 \text{ km/s}$ [15]. These processes are expected to have an increasingly significant impact as we probe into higher redshifts. The cosmic infrared background (CIRB) provides valuable insights into the star formation history of the universe [16]. This background radiation is a blend of emissions from all extragalactic sources. In the near-infrared (NIR) range, the CIRB primarily originates from stellar light, while emissions at mid- and far-infrared wavelengths are predominantly driven by the thermal radiation from cosmic dust. Several researchers have measured the near-infrared background (NIRB) in the J, K, and L bands using data from the Diffuse Infrared Background Experiment (DIRBE) aboard the Cosmic Background Explorer (COBE) satellite. More recently, Ref. ([17]) provided precise measurements of the NIRB across the 1.4 to $4 \mu\text{m}$ range using data from the near-infrared spectrometer (NIRS). A significant challenge in these measurements arises from uncertainties related to subtracting sunlight scattered by interplanetary dust (IPD). Despite this issue, some studies suggest that the observed NIRB cannot be fully explained by contributions from ordinary galaxies [18].

* k.elbourakadi@yahoo.com

† giovanni.otalora@academicos.uta.cl

A previous study [19] proposed that the earliest generation of stars, known as Population III (Pop III) stars, could contribute to the near-infrared cosmic background. Later, Ref.([20]) expanded on this idea, suggesting that a substantial portion of the unexplained near-infrared background might originate from Pop III stars. They explored a scenario with a highly top-heavy initial mass function (IMF), where stars are assumed to have masses around $300 M_{\odot}$, as indicated by recent three-dimensional simulations [21].

The exploration of the interstellar medium (ISM) in early-universe galaxies has entered an exciting phase, thanks to the remarkable capabilities of the ALMA. One of the most significant tools in this study is the $158 \mu\text{m}$ emission line associated with the $^2P_{3/2} \rightarrow ^2P_{1/2}$ fine-structure transition of ionized carbon ([C II]). This line, as the primary cooling mechanism for neutral diffuse ISM [22], is the brightest emission feature in the far-infrared spectrum [23]. Beyond the neutral diffuse gas, the [C II] line can also arise from high-density photodissociation regions (PDRs) and diffuse ionized gas, where free electrons drive the emission through collisions. While disentangling the contributions from these various gas phases can be challenging, the [C II] line remains a powerful diagnostic for studying the ISM in galaxies from the Epoch of Reionization (EoR; $z = 6 - 7$; e.g., [24]). Prior to ALMA, detections of the [C II] line at $z > 4$ were limited to galaxies with extreme star formation rates [24–26] or those hosting active galactic nuclei [27–30].

In this work we explore the transformative epoch of the Cosmic Dark Ages, detailing the universe’s progression from a neutral, lightless state to the emergence of the first stars and galaxies, driving cosmic reionization. Key topics include the role of Population III and II stars in shaping early intergalactic medium conditions, the influence of molecular hydrogen cooling on gravitational collapse, and the critical role of emission lines like Ly α and [C II] in tracing star formation, metallicity, and ISM properties. By combining theoretical models and computational simulations, the paper provides insights into the emission and spatial distribution of early stellar populations, the evolution of cosmic infrared background features, and the comparative analysis of Ly α and [C II] emission in high-redshift galaxies. This paper is subdivided as follows: in the Sec.II, we discuss the Dark Ages and the mechanisms of structure formation. In the Sec.III, we investigate Population II stars, their emission properties, and spatial distribution. Sec.IV examines Ly α and [C II] emissions as tracers of galaxy evolution during the epoch of reionization. Finally, we conclude in Sec.V, summarizing the key findings and their implications for understanding high-redshift galaxy formation and cosmic evolution.

II. THE COSMIC DARK AGES

A. The Dark Ages & Structure Formation

The Dark Ages refer to a period in the early universe that follows recombination and the universe was predominantly devoid of luminous sources. This era was marked by a neutral hydrogen-dominated intergalactic medium, with minimal radiation capable of ionizing atoms or illuminating the cosmic landscape [31]. Despite the lack luminous sources, density fluctuations seeded by quantum effects in the inflationary period grew through gravitational attraction, leading to matter clumping and the eventual formation of primordial structures [32]. As density variations in the cosmic gas and dark matter persisted, these regions with slight over-densities began the gravitational collapse, leading to galaxy formation [33]. This gravitational collapse mechanism would later lead to the formation of the first stars (Population III stars) in localized dense regions, an event prepare for the end of the Dark Ages and the start of cosmic reionization. During the Dark Ages, the IGM was primarily composed of neutral hydrogen atoms with a trace amount of helium and tiny fractions of light elements formed during Big Bang nucleosynthesis [34]. The gas temperature decreased as the universe expanded, cooling to a point where it was no longer sufficient to sustain ionized particles. This neutral state persisted throughout the Dark Ages, impacting the opacity of the medium and allowing neutral hydrogen to dominate the cosmic landscape. As outlined by Ref. ([31]), the cooling of gas through mechanisms such as hydrogen H_2 formation was essential to initiate future star formation and enabling gas clouds to fragment and collapse.

Neutral hydrogen played a critical role in shaping the spectral features during this epoch through its Lyman-alpha ($Ly\alpha$) absorption, affecting any radiation passing through the IGM. As seen in Ref. ([35]), the effective optical depth (τ_{IGM}) and higher-order Lyman series transitions was significant which imposed a blanket absorption on radiation across these wavelengths. Only wavelengths redshifted beyond the Lyman limit passed without obstruction,

marking the absorption characteristic of the Dark Ages. The scattering and reemission of photons through Lyman series contributed to faint diffuse emissions that were simulated in Ref. ([36]), the results indicate that scattered $Ly\alpha$ photons developed a characteristic asymmetric emission profile due to the IGM's Hubble expansion, creating a faint background glow that permeated the Dark Ages. The background radiation intensity observed in the cosmic infrared background (CIRB) is derived from the cumulative emissions and absorptions throughout cosmic history. Peebles' formalism [35] gives the specific intensity $I(\nu_0, z_0)$ observed at a frequency ν_0 and redshift z_0 , integrating over all redshifts $z > z_0$. For the Dark Ages, the emissivity $\epsilon(\nu, z)$ primarily reflects the IGM's thermal properties and weak emissions from non-ionizing processes:

$$I(\nu_0, z_0) = \frac{1}{4\pi} \int_{z_0}^{\infty} \epsilon(\nu, z) e^{-\tau_{IGM}(\nu_0, z_0, z)} \frac{dl}{dz} dz, \quad (1)$$

where $\frac{dl}{dz} = c [H_0 (1+z) E(z)]^{-1}$ is the line element for proper distance, governed by cosmological expansion parameters with c is the speed of light and,

$$E(z) = \sqrt{\Omega_M(1+z)^3 + \Omega_\Lambda + (1 - \Omega_M - \Omega_\Lambda)(1+z)^2}. \quad (2)$$

is the dimensionless Hubble parameter. The above form demonstrates how density fluctuations, Hubble expansion, and atomic transitions impact the observable universe's spectral features. In this context, The effective optical depth, denoted as τ_{IGM} , through the IGM is defined by [37, 38],

$$\tau_{IGM}(\nu_0, z_0, z) = \int_{z_0}^z dz' \int_0^{\infty} dN_{H_I} \zeta(N_{H_I}, z') (1 - e^{-\tau}), \quad (3)$$

where $\zeta(N_{H_I}, z') = d^2N/dN_{H_I}dz'$ represents the distribution of absorbers as a function of redshift and neutral hydrogen column density, N_{H_I} . $\tau(\nu)$ denotes the optical depth of a single cloud for ionizing radiation at frequency ν .

B. Population II Emission and Spatial Distribution

The evolution and emission properties of Population II stars are critical for understanding the cosmic timeline, especially during the early phases of galaxy formation [39]. Population II stars, characterized by low metallicity, exhibit distinct stellar and nebular emission signatures influenced by their masses, metallicities, and evolutionary stages [40]. This section presents a mathematical formalism for modeling these emissions and visualizes the spatial distribution of stars within a galaxy, based on a computational simulation. Stellar emission arises from the intrinsic radiative output of stars. For a star of mass M , metallicity Z , and age t , the effective temperature T_{eff} and luminosity L_* are modeled as[41, 42],

$$T_{eff} = 6000 \left(\frac{M}{1M_\odot} \right)^{0.5} (1 - Z), \quad (4)$$

$$L_* = M^{3.5} \exp\left(-\frac{t}{1Gyr}\right). \quad (5)$$

where the stellar emission is given by $E_* = T_{eff} \cdot L_*$ [43]. Nebular emission is driven by ionizing photons that interact with the surrounding medium [?]. The ionizing photon rate q_H scales with the stellar mass and metallicity as [45],

$$q_H = 10^{46} \left(\frac{M}{1M_\odot} \right)^{1.5} (1 - Z). \quad (6)$$

The resulting nebular emission, $E_{nebular}$ is expressed as [46],

$$E_{nebular} = c_{H_\alpha} \cdot \alpha_B \cdot q_H \cdot \frac{\exp\left(-\frac{t}{1Gyr}\right)}{1 - f_{esc}}, \quad (7)$$

where c_{H_α} represents the energy output in the H_α spectral line, α_B is the recombination coefficient for case B, which accounts for recombination events leading to photon emission in excited states, and f_{esc} denotes the fraction of ionizing photons that escape the surrounding nebula [47]. The combined emission is modeled as the sum of stellar and nebular components $E_{total} = E_* + E_{nebular}$ [47].

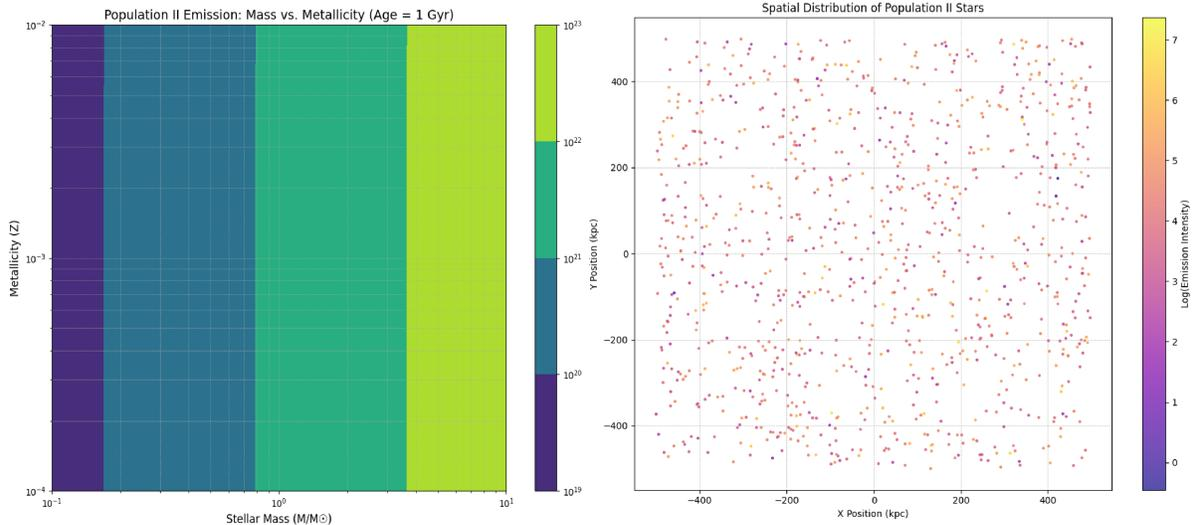


FIG. 1. Emission Intensity and Spatial Distribution of Population II Stars

Fig. 1 illustrates the emission intensity of Population II stars as a function of stellar mass (M/M_\odot) and metallicity (Z) at 1Gyr . High-mass, low-metallicity stars dominate the emission due to their high luminosity and ionizing photon production, driving stronger nebular contributions. Emission decreases for lower-mass stars and at higher metallicities due to reduced luminosity and effective temperature, resulting in a diagonal trend of peak intensity. This pattern underscores the significant role of massive, metal-poor stars in reionization and early universe enrichment. The scatter plot depicts the spatial distribution and emission intensity of Population II stars in a simulated 1kpc galaxy. High-emission stars are sparse, reflecting the rarity of massive stars, while low-emission stars dominate due to their abundance. The uniform spatial distribution indicates an isotropic placement of stars, with mixed contributions from short-lived, high-mass stars and long-lived, low-mass stars. This highlights the diversity and radiative impact of Population II stars on the light output of early galaxies.

The Dark Ages set the cosmic stage for all subsequent structure formation. The growth of matter density fluctuations into gravitationally bound structures was essential for the emergence of galaxies and clusters. This period's analytical treatment of density perturbations, the thermodynamics of the IGM, and the role of molecular hydrogen cooling are pivotal for understanding the initiation of star formation. The gravitational collapse criteria, minimum cooling thresholds, and subsequent fragmentation provide a foundation for analyzing the transition into the era of first light and cosmic reionization. This conceptual and analytical overview of the Dark Ages offers insights into the universe's silent and foundational period, paving the way for the birth of the first stars and cosmic illumination.

C. Emission and Scattering in the Cosmic Infrared Background

The Cosmic Infrared Background is shaped by the combined effects of $\text{Ly}\alpha$ photon scattering in the intergalactic medium and the emission from first-generation Population III stars [49]. $\text{Ly}\alpha$ photons emitted by these early galaxies undergo scattering interactions with the neutral hydrogen in the IGM, diffusing to longer wavelengths due to the Hubble expansion [50]. This results in an asymmetric $\text{Ly}\alpha$ emission line with a scattering profile given by [51]:

$$\Phi(\nu, z) = \begin{cases} \nu_*(z)\nu^{-2} \exp\left(-\frac{\nu_*}{\nu}\right), & \nu > 0, \\ 0, & \nu \leq 0, \end{cases} \quad (8)$$

where $\nu_*(z)$, the characteristic frequency, depends on baryonic density and cosmic expansion [51],

$$\nu_*(z) = 1.5 \times 10^{12} \text{ Hz} \left(\frac{\Omega_b h^2}{0.019} \right) \left(\frac{h}{0.7} \right)^{-1} \frac{(1+z)^3}{E(z)}, \quad (9)$$

Emission from Population III stellar clusters combines contributions from stellar spectra, nebular emissions, and Ly α line emission. The total emission spectrum is expressed as [52],

$$l_\nu(z) = \int_{M_l}^{M_u} F(\nu, M, z) \phi(M) dM, \quad (10)$$

where $F(\nu, M, z)$ includes stellar (l_ν^{star}), nebular (l_ν^{neb}), and Ly α line ($l_\nu^{\text{Ly}\alpha}$) contributions. Nebular emissions are described by [52],

$$l_\nu^{\text{neb}} = \gamma_{\text{tot}} \frac{\alpha_B}{1 - f_{\text{esc}}} q(H), \quad (11)$$

with α_B as the Case B recombination coefficient, f_{esc} the ionizing photon escape fraction, and $q(H) = Q(H)/M$ representing the ionizing photon rate per unit stellar mass. The Ly α emission, modulated by IGM scattering, is given by [53]

$$l_\nu^{\text{Ly}\alpha}(z) = c_{\text{Ly}\alpha} (1 - f_{\text{esc}}) q(H) \Phi(\nu_{\text{Ly}\alpha} - \nu, z), \quad (12)$$

where $c_{\text{Ly}\alpha}$ represents the energy output per Ly α photon. The distribution of stellar masses, defined by the Initial Mass Function (IMF), significantly impacts the emission. The Salpeter IMF ($\phi(M) \propto M^{-2.35}$) and the Larson IMF [54, 55],

$$\phi(M) \propto M^{-1} \left(1 + \frac{M}{M_c} \right)^{-1.35}, \quad (13)$$

with M_c as a characteristic mass scale, reflect differing biases toward massive stars. These processes and equations highlight the critical interplay between early star formation, photon scattering, and the evolving IGM in shaping the CIB during the cosmic dark ages.

Fig. (??) illustrates the complex behavior of Ly α emission intensity as a function of frequency and redshift, capturing how the interplay between cosmic expansion and astrophysical processes shapes the spectral energy distribution. The logarithmic frequency axis spans a wide range, from 10^{11} Hz to 10^{15} Hz , covering the typical scales where Ly α photons contribute, while the redshift extends from $z = 0.1$, representing the relatively recent universe, to $z = 10$, corresponding to the epoch of early galaxy and star formation. At high redshifts ($z \geq 5$), the intensity contours show a concentration at lower frequencies due to significant redshifting of the emitted Ly α photons. The emission intensity peaks at frequencies corresponding to the rest-frame Ly α transition redshifted by the factor $(1+z)^{-1}$, creating a strong diagonal trend in the plot. This regime reflects the dominance of primordial ionizing sources, such as early stars and galaxies, which emit photons that scatter through the surrounding intergalactic medium. For Intermediate Redshifts ($2 \leq z \leq 5$), the emission intensity exhibits a broader spread across frequencies, with a gradual weakening of the peak intensity. This broadening is attributed to the combined effects of cosmic expansion, which reduces the energy density of Ly α photons, and the partial reionization of the IGM, which alters the scattering cross-section. The contours become less sharp, indicating a smoother transition of intensity across frequencies. Finally at Low Redshift ($z \leq 2$), the contours shift further toward the low-frequency regime, with a dramatic decline in peak intensity. This reflects the universe's continued expansion, which increasingly dilutes the energy of Ly α photons, as well as the reduced contribution of new ionizing sources. The declining intensity also mirrors the reduced star

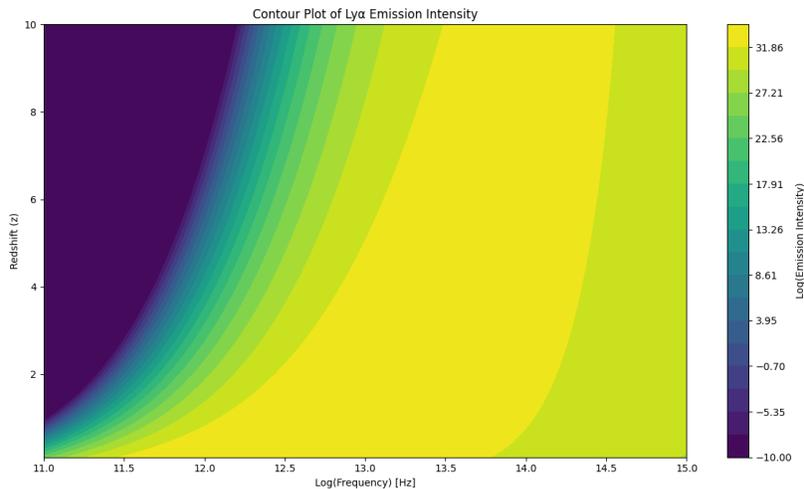


FIG. 2. Evolution of Ly α Emission Line

formation rates in the universe's late stages, contributing less to the Ly α photon population. The emission intensity drops sharply at high frequencies ($\nu \geq 10^{14} \text{ Hz}$) due to the exponential cutoff in the scattering profile $\Phi(\nu, z)$, governed by the redshift-dependent characteristic frequency $\nu_s(z)$. In the mid-range ($10^{12} \leq \nu \leq 10^{14} \text{ Hz}$), intensity varies significantly with redshift, shaped by the redshifted Ly α peak and the baryon density parameter $\Omega_b h^2$. At low frequencies ($\nu \leq 10^{12} \text{ Hz}$), intensity diminishes uniformly across redshifts due to reduced scattering efficiency, reflecting the spectral energy distribution of the ionizing sources. The results captures the Ly α emission evolution as a probe of cosmological history illustrating how early star formation epochs at high z imprint their signatures on the IGM, which are then redshifted and attenuated as the universe ages. The drop in intensity at lower redshifts highlights the diminishing role of new ionizing sources, making Ly α photons crucial tracers of reionization and large-scale structure formation.

III. [C II] EMISSION AS A METALLICITY AND STAR FORMATION TRACER

The [C II] 158 μm line serves as a powerful tracer of both metallicity and star formation in galaxies due to its origin in singly ionized carbon (C^+), a key component of the interstellar medium. Its connection to metallicity arises from the fact that carbon is produced in stars and enriched in the ISM through stellar winds and supernovae, with its abundance increasing as galaxies evolve chemically. The strength of the [C II] line depends on carbon abundance and cooling efficiency, making it particularly bright in metal-poor environments where alternative cooling mechanisms, such as CO, are less effective. Observations have demonstrated that the [C II]-to-total infrared (TIR) luminosity ratio decreases in higher metallicity regions due to dust reprocessing effects [56]. Additionally, the [C II]/CO ratio is often used to identify low-metallicity systems where CO is under-abundant [57]. As a tracer of star formation, the [C II] line is strongly linked to photodissociation regions (PDRs), where UV photons from young, massive stars heat the gas, with the subsequent emission reflecting the balance between UV heating and cooling. Empirical studies have shown a strong correlation between [C II] luminosity and star formation rate (SFR), particularly in moderate to high star formation regimes [58]. However, this relationship can be complicated in extremely dusty or metal-rich environments, where other cooling mechanisms may dominate. The far-infrared nature of the [C II] line makes it highly effective in penetrating dust, providing a clearer view of star-forming regions compared to UV or optical tracers, which are often obscured. Despite its advantages, the [C II] line can face limitations, such as saturation in dusty systems or dominance by PDR contributions, requiring additional spectral lines for contextual interpretation. Together, the [C II] line is a critical tool for understanding the chemical evolution and star formation activity of galaxies, particularly in the high-redshift universe, where it remains bright and detectable even in dust-obscured conditions [59]. The simulated [C II] intensity maps in Fig. (3) provide a valuable perspective on the evolution of galaxies across redshifts, highlighting the interconnected roles of star formation rate (SFR) and metallicity in shaping

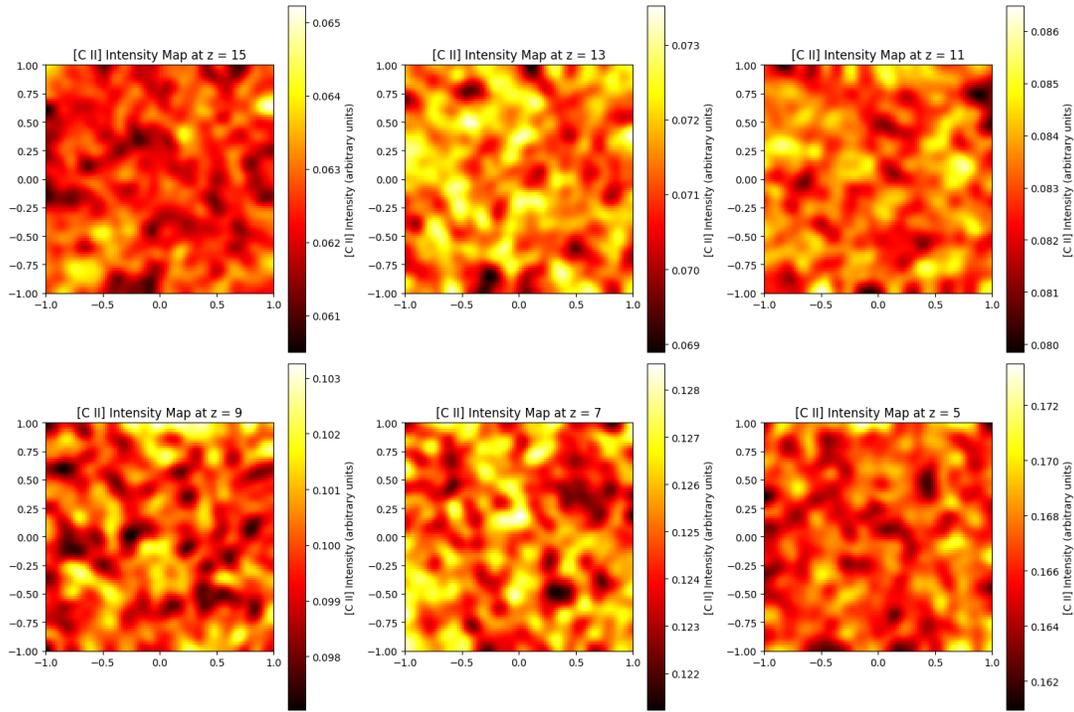


FIG. 3. [C II] Intensity across different redshifts

observed emissions, the x-axis and y-axis represent spatial coordinates on a 2D grid. At higher redshifts $z \sim 15$, the maps show weaker intensities, reflecting the early stages of galaxy formation when metallicities were lower, and the ISM was dominated by primordial gas. As redshift decreases, the simulated trend shows progressively enhanced [C II] intensities. This is driven by rising star formation rates and the enrichment of the ISM through stellar nucleosynthesis, both of which boost [C II] emission. These findings align well with observational evidence that [C II] serves as a robust tracer of star-forming regions, directly correlating with SFR and metallicity. In the simulation, metallicity influences the abundance of carbon in the ISM, which, upon ionization, produces the prominent [C II] 158 μm emission line. The maps also illustrate how cosmic evolution leads to brighter and more widespread emission, consistent with the transition from the Epoch of Reionization to the peak of star formation activity. These results are directly comparable to real observations from ALMA and JWST, which have already detected [C II] in galaxies at $z \sim 6$ and aim to push detections to $z > 10$. The use of Gaussian smoothing in the simulation accounts for observational limitations, reflecting the spatial resolution challenges faced in high-redshift studies. By connecting [C II] emission to SFR and metallicity.

The [C II] 158 μm line is a critical tool for tracing both metallicity and star formation in galaxies, particularly in the context of high-redshift studies. As it arises from singly ionized carbon C^+ , its luminosity $L_{[CII]}$ is directly linked to the carbon abundance in the interstellar medium, which scales with the galaxy's metallicity Z . This relationship can be expressed as $L_{[CII]} \propto C^+ \propto Z$, making it a reliable tracer of chemical evolution. Observationally, the [CII]–to–CO ratio, $R_{[CII]/CO} = L_{[CII]}/L_{CO}$, is often used to distinguish low-metallicity environments, as CO formation is suppressed due to insufficient dust shielding in these regions [57]. Additionally, the [C II]–to–total infrared ratio, $R_{[CII]/TIR} = L_{[CII]}/L_{TIR}$, provides insights into the cooling efficiency of carbon relative to dust reprocessing, with $R_{[CII]/TIR}$ decreasing at higher metallicities where dust dominates [56].

The [C II] line is also a valuable tracer of star formation, as it primarily originates in photodissociation regions (PDRs), where UV photons from young, massive stars heat the surrounding gas. The [C II] luminosity scales empirically with the star formation rate (SFR), often expressed as

$$SFR \left(M_{\odot} \text{yr}^{-1} \right) = \alpha \left(\frac{L_{[CII]}}{10^7 L_{\odot}} \right), \quad (14)$$

where α is a calibration constant depending on the galaxy's dust content and environment [58]. Furthermore, the balance between heating and cooling in PDRs can be quantified through the photoelectric heating efficiency ϵ is given by,

$$\epsilon = \frac{L_{[\text{CII}]} + L_{[\text{OI}]}}{L_{\text{TIR}}}, \quad (15)$$

here $L_{[\text{OI}]}$ represents the luminosity of the [O I] fine-structure line. Higher ϵ values correspond to regions of active star formation, with efficient UV heating and cooling [60]. In high-redshift galaxies, the [C II] luminosity can be observed and corrected for cosmological effects using the relationship

$$L_{[\text{CII}],\text{obs}} = \frac{L_{[\text{CII}],\text{int}}}{4\pi D_L^2 (1+z)}, \quad (16)$$

where D_L is the luminosity distance and z is the redshift. This allows for the use of [C II] as a robust tracer of star formation and metallicity in the early universe, even when traditional optical or UV tracers are obscured by dust [59]. These mathematical frameworks highlight the dual utility of the [C II] line in probing both the chemical enrichment and the star formation activity of galaxies, especially under the challenging observational conditions of the distant universe.

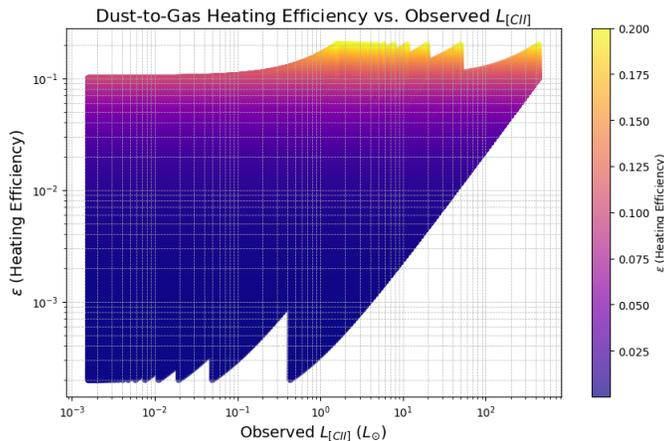


FIG. 4. Dust-to-Gas Heating Efficiency of the [C II] 158 μm line

Fig.(4) provides a detailed simulation of galaxy properties to explore the relationship between dust-to-gas heating efficiency and observed [C II] luminosity. Using intrinsic luminosities of [C II] and [OI] lines and their dependence on the total infrared luminosity L_{TIR} . The model incorporates cosmological effects by calculating the luminosity distance D_L based on the redshift and assumes a flat universe. The dust-to-gas heating efficiency relates the energy emitted in cooling lines ([C II] and [O I]) to the total infrared energy emitted by dust. Observed [C II] luminosity is derived by accounting for the term $1/D_L^2 (1+z)$, providing insights into how intrinsic properties of galaxies are altered by their distance and the expansion of the universe.

The visualization reveal the dependency of heating efficiency on cooling line emissions and their detectability. This approach mirrors observational strategies used in studies of high-redshift galaxies, such as with ALMA or JWST, to infer SFRs, ISM conditions, and dust properties. The color gradient indicates variations in heating efficiency, with brighter regions (yellow) representing higher efficiencies and darker regions (blue) representing lower efficiencies. The observed trend shows that ϵ tends to increase with increasing $L_{[\text{CII}]}$, but this relationship is not linear and exhibits significant scatter at low luminosities. This suggests that higher [CII] luminosities generally correlate with more efficient gas heating, which could reflect variations in environmental conditions, such as the density, temperature, or metallicity of the ISM. The irregularities and scatter at low luminosities may indicate complex, non-linear processes influencing the heating efficiency, possibly linked to localized star formation or the interplay of dust and gas in different regions.

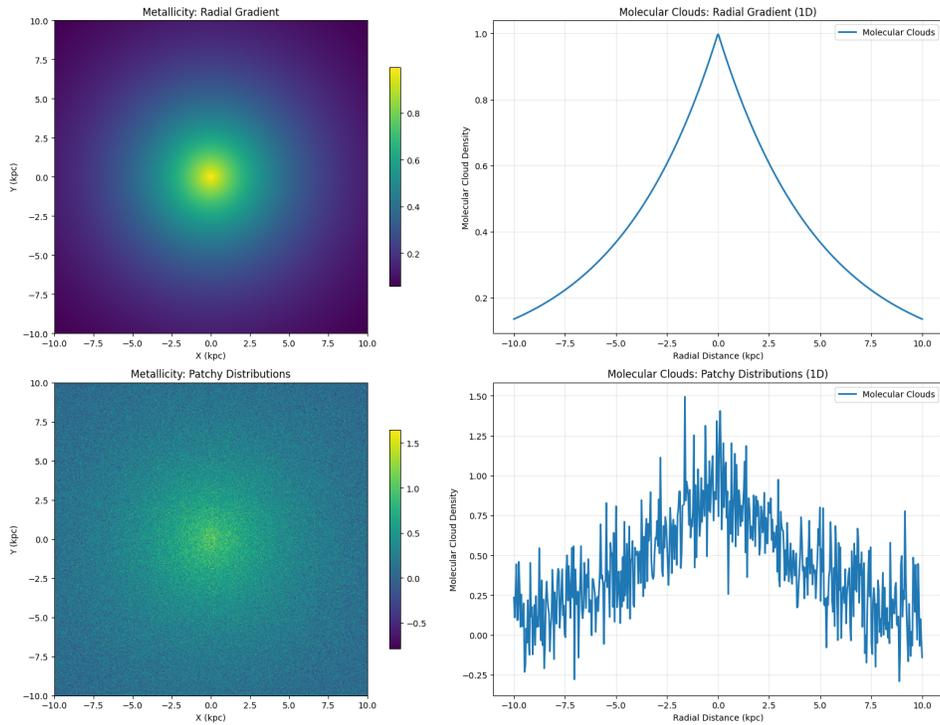


FIG. 5. Metallicity and Molecular Cloud Distributions: Radial Gradient vs. Patchy Models

Fig.(5) examines the spatial interplay between metallicity and molecular cloud distributions in galaxies through two models: the Radial Gradient and Patchy Distributions. The radial gradient model assumes an exponential decline in metallicity and molecular cloud density with radius, cloud, reflecting the enrichment of the ISM in central regions due to sustained star formation and efficient recycling of stellar materials. This model captures large-scale, axisymmetric trends, with inner regions hosting denser molecular clouds and higher metallicity, resulting in stronger [CII] emission line driven by efficient cooling and UV heating in photodissociation regions (PDRs). Conversely, the patchy distribution model introduces local stochastic variations, mimicking turbulent feedback effects such as supernova explosions and stellar winds that disrupt the ISM, creating fragmented molecular clouds and localized metallicity enhancements. This model explains the clumpy nature of [CII] emission in high-feedback environments, such as starburst regions or interacting galaxies, where molecular clouds are dynamically formed and destroyed. Together, these models describe both the global ISM behavior and localized feedback-driven variability, offering a robust framework for interpreting the spatial distribution of [CII] line emission and its connection to star formation.

IV. COMPARATIVE ANALYSIS OF $\text{Ly}\alpha$ AND [C II] IN HIGH-REDSHIFT GALAXIES

Understanding the formation and evolution of high-redshift galaxies during the epoch of reionization relies heavily on emission lines such as Lyman-alpha and [C II]. These lines serve as critical diagnostics of star formation, interstellar medium conditions, and feedback processes. $\text{Ly}\alpha$ originating from hydrogen recombination, provides insights into the ionization state of the intergalactic medium [61], while [C II], a prominent cooling line in photo-dissociation regions (PDRs), acts as a tracer of star formation and metallicity. Here, we present a theoretical framework and a computational approach to simulate these emission lines, bridging astrophysical theory and observational predictions. The observed flux $F_{\text{Ly}\alpha}$ of the $\text{Ly}\alpha$ emission line is related to the intrinsic luminosity $L_{\text{Ly}\alpha}$ by,

$$F_{\text{Ly}\alpha} = \frac{L_{\text{Ly}\alpha}}{4\pi d_L^2}, \quad (17)$$

where d_L is the luminosity distance at redshift z . In a flat $\Lambda - \text{CDM}$ cosmology is given by $d_L = (1+z) \cdot \frac{c}{H_0} \int_0^z \frac{dz'}{\sqrt{\Omega_m(1+z')^3 + \Omega_\Lambda}}$, with c as the speed of light H_0 as the Hubble constant, Ω_m and Ω_Λ as the matter and dark energy density parameters. Observations and models suggest that $L_{Ly\alpha} \propto \text{SFR}$ as $Ly\alpha$ emission scales with the ionizing photon output from young, massive stars [62, 63]. The [C II] emission line at a rest-frame frequency is a major cooling line for the ISM, especially in PDRs illuminated by young stars. The observed flux $F_{[CII]}$, depends on the intrinsic luminosity $L_{[CII]}$ and is similarly given by,

$$F_{[CII]} = \frac{L_{[CII]}}{4\pi d_L^2}. \quad (18)$$

Empirical studies, such as [64], show a correlation between $L_{[CII]}$ and SFR, indicating that $L_{[CII]} \propto \text{SFR}$. For both emission lines, the rest-frame wavelength or frequency shifts into the observed frame due to cosmological redshift,

$$\begin{aligned} \lambda_{obs} &= \lambda_{rest} \cdot (1+z), \\ \nu_{obs} &= \frac{\nu_{rest}}{1+z}. \end{aligned} \quad (19)$$

The $Ly\alpha$ falls in the near-infrared regime, while [C II] appears in the millimeter regime for high-redshift galaxies.

This study models the $Ly\alpha$ flux to decline with redshift due to increased IGM opacity, described by an attenuation factor $\exp(-\tau_{IGM})$. For [C II], the emission depends on SFR and ISM properties, with metallicity influencing the cooling efficiency.

This theoretical framework provides a path for understanding the connections between galaxy properties (SFR, metallicity, redshift) and emission line fluxes during the epoch of reionization. By focusing on intrinsic astrophysical relationships, the analysis serves as a baseline for exploring galaxy evolution and ISM conditions especially for testing hypotheses about early galaxy formation. The provided results in Fig.(6) visualizes through scatter plots

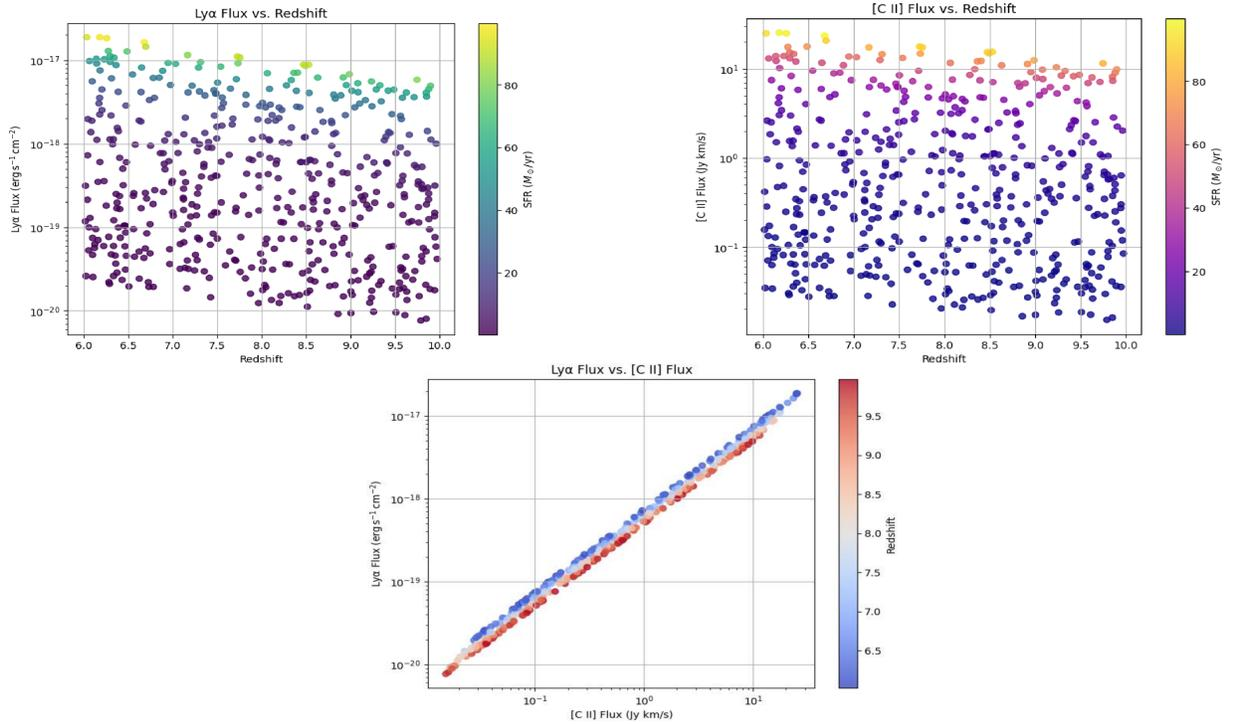


FIG. 6. Metallicity and Molecular Cloud Distributions: Radial Gradient vs. Patchy Models

the relationship between fluxes, redshifts, and SFRs to simulate the theoretical emission properties of high-redshift galaxies during the epoch of reionization, focusing on the $Ly\alpha$ and [C II] lines. Using a flat Λ -CDM cosmology, the

code predicts the fluxes of these lines for galaxies with redshifts ranging from $z \sim 6$ to $z \sim 10$ and star formation rates (SFRs) spanning 0.1 to $100 M_{\odot} \text{yr}^{-1}$. The $\text{Ly}\alpha$ flux is modeled as inversely proportional to the square of the luminosity distance, with attenuation due to the intergalactic medium (IGM). The [C II] flux is similarly scaled, incorporating its dependence on SFR and redshift, while assuming a simplified metallicity factor. The flux decreases with increasing redshift, primarily due to the growing optical depth of the IGM, which attenuates the emission. Conversely, the [C II] flux remains more stable, as it is less affected by the IGM and directly tied to the SFR and ISM conditions. Moreover, the $\text{Ly}\alpha$ line, is redshifted into the near-infrared, while the [C II] line shifts into the millimeter range. These shifts follow the cosmological redshift relations and enable the placement of these lines in observational spectra for high-redshift galaxies. The [C II] flux calculation assumes a uniform metallicity, emphasizing its theoretical dependence on SFR alone, the results helps understanding of how $\text{Ly}\alpha$ and [C II] emission lines trace galaxy properties in the early universe, serving as a highlight the distinct roles of these lines in probing galaxy evolution during cosmic history.

V. CONCLUSION

This paper aims to explore the critical processes and observational signatures of the Cosmic Dark Ages, focusing on the transition from a neutral, dark universe to one illuminated by the first stars and galaxies. By leveraging theoretical models and simulations, the study examines how key emission lines such as $\text{Ly}\alpha$ and [C II] $158 \mu\text{m}$ trace star formation, metallicity, and intergalactic medium conditions, providing insights into the epoch of reionization. Firstly, we examined the spatial and emission profiles reveal the dominance of high-mass, low-metallicity stars in driving nebular emissions and radiative output during the early stages of galaxy formation. The simulated spatial distributions underscore the rarity of massive stars but highlight their critical role in reionization and enriching the IGM. On the other hand, the evolution of $\text{Ly}\alpha$ emission intensity across redshifts and frequencies captures the interplay between cosmic expansion and photon scattering in the IGM. At high redshifts, the sharp contours of $\text{Ly}\alpha$ emission reflect the influence of primordial ionizing sources, while at lower redshifts, the emission weakens due to declining star formation rates and IGM transparency. Moreover, the [C II] intensity maps and their connection to star formation and metallicity emphasize the line's effectiveness in probing galaxy properties. The results demonstrate the evolution of [C II] emission from weak, localized regions in low-metallicity environments to brighter, widespread emissions as galaxies evolve chemically. Furthermore, the relationship between [C II] luminosity, star formation rates, and dust-to-gas heating efficiency provides a comprehensive view of the ISM's radiative cooling processes. These results align with observational trends, reinforcing the role of [C II] as a reliable tracer of early star-forming galaxies. Then, further investigations shows that the radial gradient and patchy distribution models highlight the dual influence of large-scale ISM enrichment and localized feedback-driven variability on [C II] emissions. These models capture the balance between steady enrichment processes and stochastic feedback effects, providing a framework for interpreting emission line clumpiness in high-redshift galaxies. Finally, the contrasting behaviors of $\text{Ly}\alpha$ and [C II] fluxes across redshifts reveal their complementary roles in tracing early galaxy properties. While $\text{Ly}\alpha$ is highly sensitive to IGM opacity and declines sharply with redshift, [C II] remains stable and directly correlates with star formation and metallicity. Overall, this study bridges theoretical predictions with simulation, offering a robust framework for interpreting high-redshift galaxy evolution. The findings provide valuable guidance for upcoming observations enhancing our understanding of the universe's transition from the Cosmic Dark Ages to the era of reionization.

VI. ACKNOWLEDGMENTS

G. Otalora acknowledges Dirección de Investigación, Post-grado y Transferencia Tecnológica de la Universidad de Tarapacá for financial support through Proyecto UTA Mayor 4737-24.

[1] Carilli, C. L., Murphy, E. J., Ferrara, A., & Dayal, P. (2017). *Galaxies into the Dark Ages*. The Astrophysical Journal, 848(1), 49.

- [2] Collaboration, P., Arnaud⁶⁷, M., Ashdown⁶³, M., Atrio-Barandela¹⁷, F., Aumont⁵⁴, J., Baccigalupi⁸², C., ... & Morgante⁴⁵, G. (2016). *Planck intermediate results*. A&A, 586, A134.
- [3] Bañados, E., Venemans, B. P., Decarli, R. O. B. E. R. T. O., Farina, E. P., Mazzucchelli, C., Walter, F., ... & Yang, Q. (2016). *The Pan-STARRS1 distant $z > 5.6$ quasar survey: more than 100 quasars within the first Gyr of the Universe*. The Astrophysical Journal Supplement Series, 227(1), 11.
- [4] Ouchi, M., Ono, Y., & Shibuya, T. (2020). *Observations of the Lyman- α Universe*. Annual Review of Astronomy and Astrophysics, 58(1), 617-659.
- [5] Parsons, A. R., Liu, A., Aguirre, J. E., Ali, Z. S., Bradley, R. F., Carilli, C. L., ... & Walbrugh, W. P. (2014). *New limits on 21 cm epoch of reionization from paper-32 consistent with an x-ray heated intergalactic medium at $z = 7.7$* . The Astrophysical Journal, 788(2), 106.
- [6] Ali, Z. S., Parsons, A. R., Zheng, H., Pober, J. C., Liu, A., Aguirre, J. E., ... & Walker, A. (2015). *64 constraints on reionization: the 21 cm power spectrum at $z = 8.4$* . The Astrophysical Journal, 809(1), 61.
- [7] Fan, X., Strauss, M. A., Richards, G. T., Hennawi, J. F., Becker, R. H., White, R. L., ... & Voges, W. (2006). *A survey of $z > 5.7$ quasars in the sloan digital sky survey. IV. Discovery of seven additional quasars*. The Astronomical Journal, 131(3), 1203.
- [8] Robertson, B. E., Ellis, R. S., Furlanetto, S. R., & Dunlop, J. S. (2015). *Cosmic reionization and early star-forming galaxies: A joint analysis of new constraints from Planck and the Hubble Space Telescope*. The Astrophysical Journal Letters, 802(2), L19.
- [9] Greig, B., & Mesinger, A. (2017). *The global history of reionization*. Monthly Notices of the Royal Astronomical Society, 465(4), 4838-4852.
- [10] Pope, A., & Chary, R. R. (2010). *SEARCHING FOR THE HIGHEST REDSHIFT SOURCES IN 250–500 μm SUBMILLIMETER SURVEYS*. The Astrophysical Journal Letters, 715(2), L171.
- [11] Dayal, P., Ferrara, A., Dunlop, J. S., & Pacucci, F. (2014). *Essential physics of early galaxy formation*. Monthly Notices of the Royal Astronomical Society, 445(3), 2545-2557.
- [12] Topping, M. W., & Shull, J. M. (2015). *The efficiency of stellar reionization: effects of rotation, metallicity, and initial mass function*. The Astrophysical Journal, 800(2), 97.
- [13] Yue, B., Ferrara, A., Pallottini, A., Gallerani, S., & Vallini, L. (2015). *Intensity mapping of [C II] emission from early galaxies*. Monthly Notices of the Royal Astronomical Society, 450(4), 3829-3839.
- [14] Mashian, N., Oesch, P. A., & Loeb, A. (2016). *An empirical model for the galaxy luminosity and star formation rate function at high redshift*. Monthly Notices of the Royal Astronomical Society, 455(2), 2101-2109.
- [15] Castellano, M., Dayal, P., Pentericci, L., Fontana, A., Hutter, A., Brammer, G., ... & Wagg, J. (2016). *First observational support for overlapping reionized bubbles generated by a galaxy overdensity*. The Astrophysical Journal Letters, 818(1), L3.
- [16] Hauser, M. G., & Dwek, E. (2001). *The cosmic infrared background: measurements and implications*. Annual Review of Astronomy and Astrophysics, 39(1), 249-307.
- [17] Matsumoto, H., Tsuru, T. G., Fukazawa, Y., Hattori, M., & Davis, D. S. (2000). *Gas, iron, and gravitational mass in galaxy clusters: The general lack of cluster evolution at $z < 1.0$* . Publications of the Astronomical Society of Japan, 52(1), 153-160.
- [18] Totani, T., Yoshii, Y., Iwamuro, F., Maihara, T., & Motohara, K. (2001). *Diffuse extragalactic background light versus deep galaxy counts in the subaru deep field: missing light in the universe?*. The Astrophysical Journal, 550(2), L137.
- [19] Bond, J. R., Carr, B. J., & Hogan, C. J. (1986). *Spectrum and anisotropy of the cosmic infrared background*. Astrophysical Journal, Part 1 (ISSN 0004-637X), vol. 306, July 15, 1986, p. 428-450., 306, 428-450.
- [20] Santos, M. R., Bromm, V., & Kamionkowski, M. (2002). *The contribution of the first stars to the cosmic infrared background*. Monthly Notices of the Royal Astronomical Society, 336(4), 1082-1092.
- [21] Bromm, V., Coppi, P. S., & Larson, R. B. (2002). *The formation of the first stars. I. The primordial star-forming cloud*. The Astrophysical Journal, 564(1), 23.
- [22] Wolfire, M. G., McKee, C. F., Hollenbach, D., & Tielens, A. G. G. M. (2003). *Neutral atomic phases of the interstellar medium in the galaxy*. The Astrophysical Journal, 587(1), 278.
- [23] Stacey, G. J., Geis, N., Genzel, R., Lugten, J. B., Poglitsch, A., Sternberg, A., & Townes, C. H. (1991). *The 158 micron C II line-A measure of global star formation activity in galaxies*. Astrophysical Journal, Part 1 (ISSN 0004-637X), vol. 373, June 1, 1991, p. 423-444. Previously announced in STAR as N91-16977., 373, 423-444.
- [24] Carilli, C. L., & Walter, F. (2013). *Cool gas in high-redshift galaxies*. Annual Review of Astronomy and Astrophysics, 51(1), 105-161.
- [25] Carniani, S., Marconi, A., Biggs, A., Cresci, G., Cupani, G., D'Odorico, V., ... & Zwaan, M. A. (2013). *Strongly star-forming rotating disks in a complex merging system at $z = 4.7$ as revealed by ALMA*. Astronomy & Astrophysics, 559, A29.
- [26] De Breuck, C., Williams, R. J., Swinbank, M., Caselli, P., Coppin, K., Davis, T. A., ... & Zwaan, M. A. (2014). *ALMA resolves turbulent, rotating [CII] emission in a young starburst galaxy at $z = 4.8$* . Astronomy & Astrophysics, 565, A59.
- [27] Maiolino, R., Cox, P., Caselli, P., Beelen, A., Bertoldi, F., Carilli, C. L., ... & Walter, F. (2005). *First detection of [CII] 158 μm at high redshift: vigorous star formation in the early universe*. Astronomy & Astrophysics, 440(2), L51-L54.
- [28] Maiolino, R., Gallerani, S., Neri, R., Cicone, C., Ferrara, A., Genzel, R., ... & Piconcelli, E. (2012). *Evidence of strong quasar feedback in the early Universe*. Monthly Notices of the Royal Astronomical Society: Letters, 425(1), L66-L70.

- [29] Venemans, B. P., McMahon, R. G., Walter, F., Decarli, R., Cox, P., Neri, R., ... & Warren, S. J. (2012). *Detection of atomic carbon [C ii] 158 μ m and dust emission from a $z = 7.1$ quasar host galaxy*. The Astrophysical Journal Letters, 751(2), L25.
- [30] Cicone, C. L. A. U. D. I. A., Maiolino, R., Gallerani, S., Neri, R., Ferrara, A., Sturm, E., ... & Feruglio, C. (2015). *Very extended cold gas, star formation and outflows in the halo of a bright quasar at $z > 6$* . Astronomy & Astrophysics, 574, A14.
- [31] Salvaterra, R., & Ferrara, A. (2003). *The imprint of the cosmic dark ages on the near-infrared background*. Monthly Notices of the Royal Astronomical Society, 339(4), 973-982.
- [32] Casey, C. M., Zavala, J. A., Spilker, J., Da Cunha, E., Hodge, J., Hung, C. L., ... & Drew, P. (2018). *The brightest galaxies in the dark ages: galaxies' dust continuum emission during the reionization era*. The Astrophysical Journal, 862(1), 77.
- [33] McGaugh, S. S. (2021). *Testing galaxy formation and dark matter with low surface brightness galaxies*. Studies in History and Philosophy of Science, 88, 220-236.
- [34] Monsalve, R. A., Altamirano, C., Bidula, V., Bustos, R., Bye, C. H., Chiang, H. C., ... & Thyagarajan, N. (2024). *Mapper of the IGM spin temperature: instrument overview*. Monthly Notices of the Royal Astronomical Society, 530(4), 4125-4147.
- [35] Peebles, P. J. E. (1993). *Principles of physical cosmology* (Vol. 27). Princeton university press.
- [36] Loeb, A., & Rybicki, G. B. (1999). *Scattered Ly α radiation around sources before cosmological reionization*. The Astrophysical Journal, 524(2), 527.
- [37] Madau, P. (1992). *The contribution of quasars to the ultraviolet extragalactic background*. Astrophysical Journal, Part 2-Letters (ISSN 0004-637X), vol. 389, April 10, 1992, p. L1-L4., 389, L1-L4.
- [38] Madau, P. (1991). *QSO absorption systems and the origin of the ionizing background at high redshift*. Astrophysical Journal, Part 2-Letters (ISSN 0004-637X), vol. 376, Aug. 1, 1991, p. L33-L36., 376, L33-L36.
- [39] Bromm, V., & Larson, R. B. (2004). *The first stars*. Annu. Rev. Astron. Astrophys., 42(1), 79-118.
- [40] Schneider, R., Omukai, K., Inoue, A. K., & Ferrara, A. (2006). *Fragmentation of star-forming clouds enriched with the first dust*. Monthly Notices of the Royal Astronomical Society, 369(3), 1437-1444.
- [41] Vogelsberger, M., Marinacci, F., Torrey, P., & Puchwein, E. (2020). *Cosmological simulations of galaxy formation*. Nature Reviews Physics, 2(1), 42-66.
- [42] Anderson, R. I., Ekström, S., Georgy, C., Meynet, G., Mowlavi, N., & Eyer, L. (2014). *On the effect of rotation on populations of classical Cepheids-I. Predictions at solar metallicity*. Astronomy & Astrophysics, 564, A100.
- [43] Kippenhahn, R., Weigert, A., & Weiss, A. (1990). *Stellar structure and evolution* (Vol. 192). Berlin: Springer-verlag.
- [44] Osterbrock, D. E., & Ferland, G. J. (2006). *Astrophysics Of Gas Nebulae and Active Galactic Nuclei*. University science books.
- [45] Simón-DÁaz, S., & Stasińska, G. (2008). *The ionizing radiation from massive stars and its impact on H ii regions: results from modern model atmospheres*. Monthly Notices of the Royal Astronomical Society, 389(3), 1009-1021.
- [46] Dopita, M. A., & Sutherland, R. S. (1995). *Spectral signatures of fast shocks. II. Optical diagnostic diagrams*. Astrophysical Journal v. 455, p. 468, 455, 468.
- [47] Rybicki, G. B., & Lightman, A. P. (2024). *Radiative processes in astrophysics*. John Wiley & Sons.
- [48] Charlot, S., & Fall, S. M. (2000). *A simple model for the absorption of starlight by dust in galaxies*. The Astrophysical Journal, 539(2), 718.
- [49] Barkana, R., & Loeb, A. (2001). *In the beginning: the first sources of light and the reionization of the universe*. Physics reports, 349(2), 125-238.
- [50] Loeb, A., & Furlanetto, S. R. (2013). *The first galaxies in the universe*. Princeton University Press.
- [51] Pritchard, J. R., & Loeb, A. (2012). *21 cm cosmology in the 21st century*. Reports on Progress in Physics, 75(8), 086901.
- [52] Schaerer, D. (2002). *On the properties of massive Population III stars and metal-free stellar populations*. Astronomy & Astrophysics, 382(1), 28-42.
- [53] Dopita, M. A., & Sutherland, R. S. (1995). *Spectral signatures of fast shocks. II. Optical diagnostic diagrams*. Astrophysical Journal v. 455, p. 468, 455, 468.
- [54] Larson, R. B. (1998). *Early star formation and the evolution of the stellar initial mass function in galaxies*. Monthly Notices of the Royal Astronomical Society, 301(2), 569-581.
- [55] Bromm, V., & Yoshida, N. (2011). *The first galaxies*. Annual Review of Astronomy and Astrophysics, 49(1), 373-407.
- [56] De Looze, I., Baes, M., Bendo, G. J., Cortese, L., & Fritz, J. (2011). *The reliability of [C II] as an indicator of the star formation rate*. Monthly Notices of the Royal Astronomical Society, 416(4), 2712-2724.
- [57] Pineda, J. L., Langer, W. D., Velusamy, T., & Goldsmith, P. F. (2013). *A Herschel [C ii] Galactic plane survey-I. The global distribution of ISM gas components*. Astronomy & Astrophysics, 554, A103.
- [58] Stacey, G. J., Hailey-Dunsheath, S., Ferkinhoff, C., Nikola, T., Parshley, S. C., Benford, D. J., ... & Fiolet, N. (2010). *A 158 μ m [C II] line survey of galaxies at $z \sim 1 - 2$: an indicator of star formation in the early universe*. The Astrophysical Journal, 724(2), 957.
- [59] Carilli, C. L., & Walter, F. (2013). *Cool gas in high-redshift galaxies*. Annual Review of Astronomy and Astrophysics, 51(1), 105-161.
- [60] Hollenbach, D. J., & Tielens, A. G. G. M. (1999). *Photodissociation regions in the interstellar medium of galaxies*. Reviews of Modern Physics, 71(1), 173.

- [61] Hu, W., Wang, J., Infante, L., Rhoads, J. E., Zheng, Z. Y., Yang, H., ... & Zheng, X. (2021). *A Lyman- α protocluster at redshift 6.9*. *Nature Astronomy*, 5(5), 485-490.
- [62] Kennicutt Jr, R. C. (1998). *Star formation in galaxies along the Hubble sequence*. *Annual Review of Astronomy and Astrophysics*, 36(1), 189-231.
- [63] Madau, P., & Dickinson, M. (2014). *Cosmic star-formation history*. *Annual Review of Astronomy and Astrophysics*, 52(1), 415-486.
- [64] De Looze, I., Cormier, D., Leboutteiller, V., Madden, S., Baes, M., Bendo, G. J., ... & Sturm, E. (2014). *The applicability of far-infrared fine-structure lines as star formation rate tracers over wide ranges of metallicities and galaxy types*. *Astronomy & Astrophysics*, 568, A62.